

CHAPTER 3
PRINCIPLES OF ELECTRICAL CAPACITANCE TOMOGRAPHY
AND DIFFERENTIAL PRESURE FOR VOID FRACTION
MEASUREMENTS

3.1 Introduction

The idea of *Process Tomography* was evolved in mid-1980's that led to the present generation of process tomography systems. The word tomography mainly originates from two Greek words; tomos meaning "to slice" and graphia meaning "description/image". The basic aim of modern tomography is to determine or exploring the distribution of materials in some region of interest by obtaining a set of measurements using sensors that are distributed around the periphery [53]. In medical applications, the contrasting material may be normal or cancerous tissue, and for industrial applications the material could be gas, oil or water in a pipeline. Tomographic measurements are 'non-intrusive', penetrating the wall of the sensor but not entering into the medium, and also, ideally 'non-invasive', the sensors are located on the outer periphery of the wall [5]. The need for tomography is equivalent to medical need for body scanners, which has been met by the computer-aided tomography.

Industrial processes tend to be complex in nature. In process application, the choice of using a particular tomography modality depends on the nature of flow under investigation, the information about the process, the size of the process vessel, and the environment of the process operation [54]. The ample scope of tomographic techniques and the problems associated with each modality makes this field essentially interdisciplinary.

Process tomography can be used to obtain both qualitative and quantitative data needed in modelling a multi-fluid flow system. For instance, different flow patterns are characterized, in a qualitative way. Secondly, a process model verification of a qualitative model is based on comparison of calculated fields of void fraction or velocities with measurement results [5]. Hence, process tomography provides a novel means of visualising the internal behaviour of industrial processes. The cross-sectional images produced by tomography systems provide valuable information on the process, which can be further used for visualisation and monitoring [55]. A particularly successful approach for industrial applications involves electrical tomography. It is based on the measurement of electrical properties through the utilization of the capacitive (ECT), resistive (ERT) or inductive (EIT) nature of the flow under investigation. One tomographic measurement technique that is well suited to both research and industrial applications and has been focussed in this dissertation is the *electrical capacitance tomography* (ECT).

Electrical capacitance sensors provide a fully non-intrusive way to measure the average void fraction over a given volume of a two-phase mixture. However, the impedance measurement technique is a practical and cost-effective method for void fraction measurement. There are, however, several disadvantages also, for example, the capacitance measurement is sensitive to the void fraction distribution or flow regimes due to the non-uniformity of the electric field inside the measuring domain. This however, can be compensated by identifying the flow pattern [3].

The advantages of ECT have involved scientific researchers and industry to carry out the research into it and use it as an imaging tool to visualize the dielectric distribution of multiphase processes [4]. Table 3.1 reviewed the some significant advantages and disadvantages of ECT, ERT and EIT measurement techniques.

Table 3.1: Characteristics of ECT, ERT and EIT

No.	Tech-nique	Advantages	Disadvantages
1	ECT	No radiation, rapid response, low cost, non-intrusive and non-invasive	Issue of stray capacitance and limited to measure oil mixture
2	ERT	Provide 2D and 3D flow, phase distribution can be reconstructed	Low measurement precision but it is feasible to find precise method
3	EIT	Simple and inexpensive	Inaccurate for stratified or intermittent flow in a horizontal channel

3.2 ECT Measurement System

ECT technology has been developed for imaging industrial processes containing dielectric materials. It is based on measuring the changes in capacitance that are caused by the change in dielectric material distribution. It is a newly developed technique for finding out the internal fluid flow characteristics and provides the quantitative measures of flow which is used for image and flow rate information [56]. ECT system mainly comprises of three main components: (1) a capacitance sensor as shown in Figure 3.1 (a), (2) data acquisition system as shown in Figure 3.1 (b) and (3) control computer for reconstruction as shown in Figure 3.1 (c).

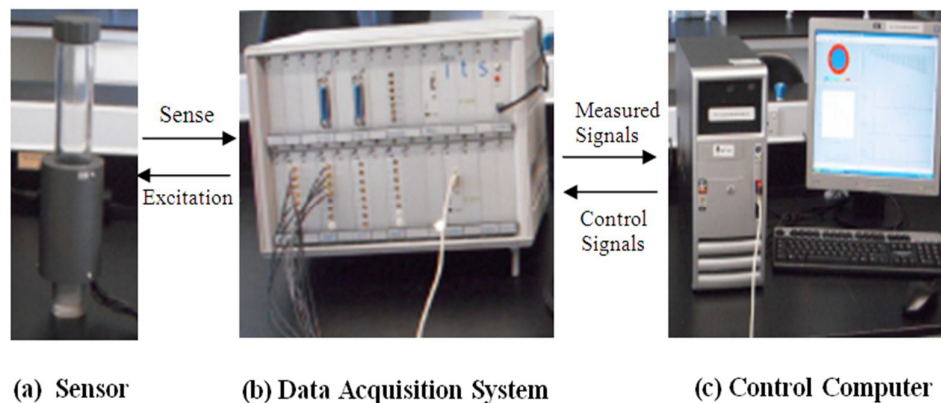


Figure 3.1: Basic ECT System.

a) *ECT Sensor*

The sensor consists of an array of electrodes attached to the periphery of the pipe which is to be imaged. The electrodes can be symmetrically mounted outside or inside of an insulating pipe. Figure 3.2 shows a cross-sectional view of a 12 electrodes ECT sensor. The electrodes are connected to the data acquisition system by short lengths of co-axial cable to reduce the effect of extraneous environmental noise and interference [57].

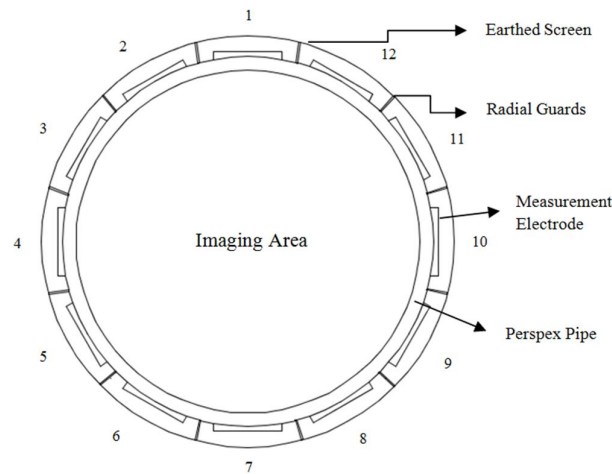


Figure 3.2: Cross-sectional View of Typical ECT Sensor with 12 External Electrodes [4].

b) *Data Acquisition System*

The data acquisition unit is used for sequential sampling of electrodes and measures the capacitance for all possible electrode combinations. The capacitance measuring unit as shown in Figure 3.1 (b) constitutes of the necessary electronic circuitry to measure and condition the signals received from the capacitance sensor [57].

c) *Control Computer*

The computer system has two major functions. Firstly, it controls the measurement operations performed by sensing electronics, and secondly it uses the measurement data to reconstruct the tomographic images [57].

3.2.1 Capacitance Measurement Principle

The ECT sensor cross-sectional model as previously shown in Figure 3.2 is composed of 12 copper plates which are installed on the outer periphery of the pipe. There is a radial grounding plate between two adjacent electrodes for reducing the adjacent electrodes capacitance value. It is acted as a grounded screen for shielding the entire system and also making it not to interfere from stray fields [58], [59]. The 12 electrode system as shown in Figure 3.2 is numbered and excited by an electric potential in an increasing order. The basic capacitance measurement principle used in ECT is shown in Figure 3.3. In tomography, the object to be imaged is surrounded by electrodes, which acts as both sources and detectors. The electrodes are excited one by one, or in pairs depending on the protocol used.

There are number of protocols used in ECT measurements but *Protocol 1* is the most widely used in data acquisition systems for ECT. According to this protocol, only one electrode is excited at any point in time and the remaining electrodes are kept at ground potential and function as detectors until the measurement completes the full cycle or N-1 electrodes [60].

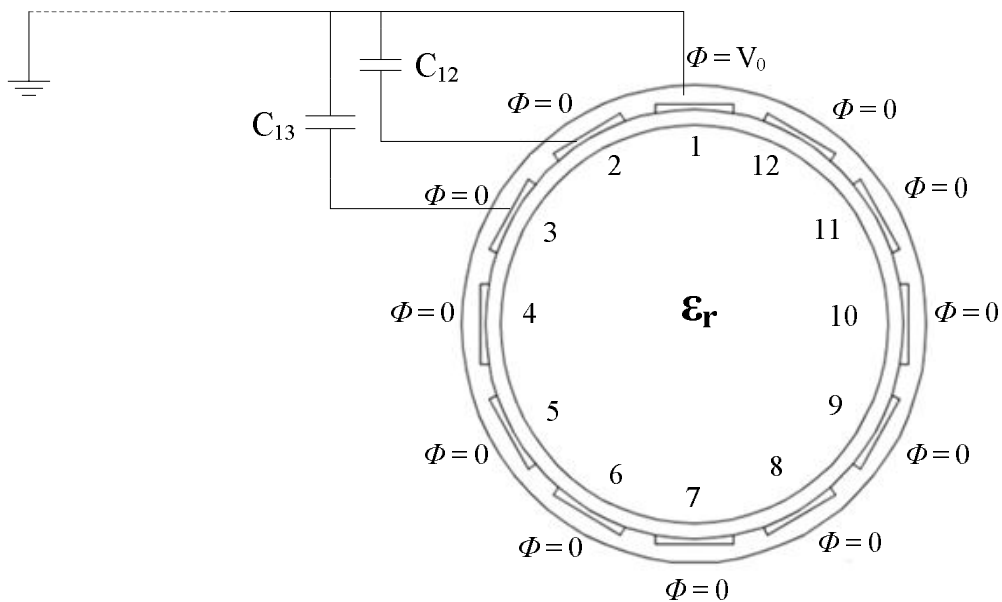


Figure 3.3: Schematic Representation of the Measurement Principle of an ECT System [59].

During a measurement period, each electrode in an ECT sensor is energised by applying an excitation voltage signal, and the induced charge/current is detected from all other electrodes while their potential is kept at zero. For example, in the first step, to obtain a complete set of data for one image, electrode 1 is used for excitation by applying a potential and electrode 2-12 for detection as they connected to the virtual ground terminals, so that they remain at zero potential with respect to the ground, obtaining 11 capacitance measurements. In the next step, electrode 2 is excited whereas, electrodes 3-12 are kept at ground potential for detection, obtaining ten capacitance measurements. This process continues until electrode N-1 i.e. electrode 11 is excited and electrode 12 is used for detection, obtaining only one capacitance measurement. In this way, there will be 66 independent capacitance measurements, which is governed by the following equation [61]:

$$M = \frac{N(N-1)}{2} \quad (3-1)$$

where, M is independent inter-electrode capacitance measurement and N is the number of electrodes located around the circumference. Figure 3.4 indicates the 66 different combinations for 12 electrodes sensor.

The measurements of these capacitances are dependent on the geometry of the electrodes and once the size and location of electrodes are determined, the permittivity distribution $\epsilon(x, y)$ is known [62]. The actual capacitance changes measured will be very small, in the order of *pico* or *femto* Farad (10^{-12} F or 10^{-15} F).

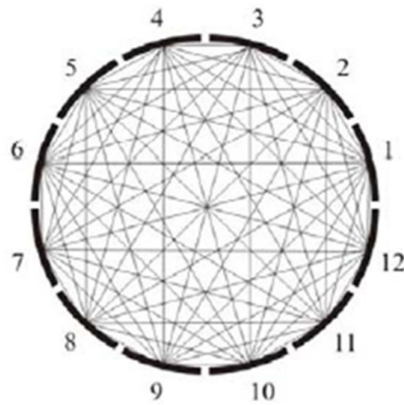


Figure 3.4: 66 Measurement Combinations for 12 Electrodes Sensor [4].

3.2.2 Factors Affecting Capacitance Measurement

The capacitance can be defined as the magnitude of charges (Q) on both electrodes divided by the potential difference (V) between the electrodes. Capacitance is also defined as a function of distance between two electrodes (d), area of the plate (A_{plate}) and the constant of the dielectric (ϵ_r) and free space (ϵ_0). The mathematical representation of two definitions is shown in equation (3-2) and (3-3) [63]:

$$C = \frac{Q}{V} \quad (3-2)$$

The simplest capacitance sensor consists of two parallel metal plates separated by a distance d as shown in Figure 3.5 and mathematically expressed in equation (3-3) [63]:

$$C = \frac{\epsilon_0 \epsilon_r A_{plate}}{d} \quad (3-3)$$

where, ϵ_0 is the dielectric constant of free space (8.85 pFm^{-1}), ϵ_r is the permittivity of the material, A_{plate} is the area of the capacitive plate (m^2) and d is the spacing between the two plates (m).

Any insulator placed between the plates will cause the capacitance increase by a particular factor. The factor by which the capacitance is increased is the “*relative permittivity*” of the material between plates. Permittivity is defined as the material’s ability to “*permit*” an electric field [63].

Equation (3-3) implies a simple relationship that capacitance is proportional to permittivity. However, the geometry of an ECT sensor is not so simple like that of a parallel plate sensor and the permittivity distribution is generally not uniform. ECT sensor has to be designed to meet certain criteria in order to get a good performance. The concept of ECT is also based on the capacitance and permittivity distribution of the medium within the vessel / pipe. Since the permittivity of each measured element is a constant, the measured element can be identified by knowing the capacitance / voltage between the electrodes.

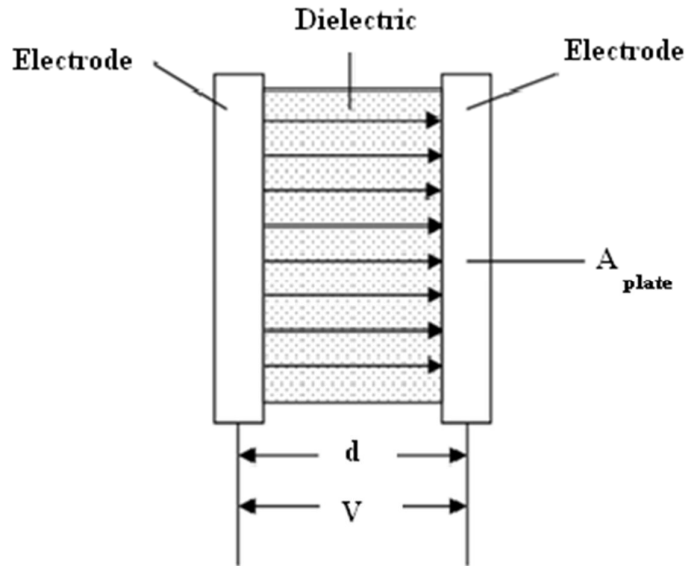


Figure 3.5: Electric Charge and Voltage of Capacitor.

3.2.3 ECT Sensor Characteristics

In most applications, the electrodes of an ECT sensor are placed on the outer periphery of the vessel or pipe. To ensure a good performance of an ECT sensor various design parameters need to be considered that meet the requirements for any industrial application such as:

- i. Low noise level
- ii. Wide dynamic measurement range
- iii. High immunity to stray capacitance
- iv. Fast data capture rate

There are many issues that are related to ECT sensor design. Among them, the most common are [61]:

- 1) Electrodes location
- 2) Number of electrodes

- 3) Length of electrodes
- 4) Driven guard electrodes
- 5) Earthed screens
- 6) Sensor simulation

3.2.3.1 Electrodes Location

If the vessel wall is non-conducting, capacitance electrodes can be located in two possible ways, one is outside and the other is inside. It is common to mount the measurement electrodes outside an insulating frame because in this case, ECT sensor is non-invasive and non-intrusive, a feature that is desired by an industry. The convention used to identify the electrodes is to number them anticlockwise [64]. This work mainly focuses on the application of external mounted electrodes.

Capacitance sensors with circular cross-section are surrounded by an array of equally spaced electrodes with an outer earthed screen as shown in Figure 3.6 (a). An alternative arrangement is to fit the electrodes inside the vessel as shown in Figure 3.6 (b). Each arrangement has some advantages and disadvantages which are summarised in Table 3.2 [65].

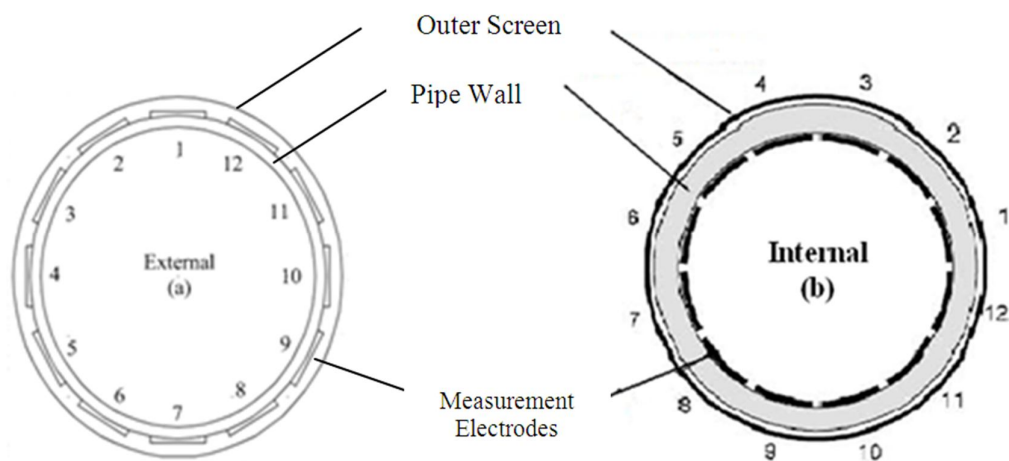


Figure 3.6: Cross-Section of Sensor with (a) External & (b) Internal Electrodes [60].

Table 3.2: Characteristics of External and Internal Electrodes

Type of electrodes	Advantages	Disadvantages
External	<ul style="list-style-type: none">• Small standing capacitance• No contact to process• Low cost• Easy to construct	<ul style="list-style-type: none">• Pipe wall capacitance effect• Large standing capacitance
Internal	<ul style="list-style-type: none">• High sensitivity• Small standing capacitance• No pipe wall capacitance effect	<ul style="list-style-type: none">• Contact to process• Difficult to prevent leakage• Difficult to construct

3.2.3.2 Number of Electrodes

The number of electrodes is the main concern in designing of an ECT sensor. By using a small number of electrodes, following advantages are expected [61]:

- i. Simplifying hardware (less data acquisition channels are required)
- ii. Faster data acquisition rate expected
- iii. Length of electrodes can reduce because inter-electrode capacitance is proportional to the size of electrodes.

The number of independent capacitance measurements is small for smaller number of electrodes, and therefore a good image cannot be found. Table 3.3 gives some numerical values for the number of electrodes that are found by using the equation (3-1). However, with the increased number of electrodes, the number of independent capacitance measurements increases that may improve the image resolution.

TABLE 3.3: Relationships between Number of Electrodes and Number of Independent Capacitance Measurement

Number of electrodes (N)	Number of independent capacitance measurement (M)
6	15
8	28
12	66
16	120

However, there are some difficulties in selecting an increased number of electrodes which are defined as follows [61]:

- i. Complicated and expensive hardware
- ii. Slower data acquisition rate because of more measurements to be taken
- iii. Smaller capacitance to be measured.

Therefore, there is a trade-offs in considering the number of electrodes. Commonly, 8 or 12 electrodes are used for ECT sensor. The number of electrodes used depends on the inter-electrode capacitance values and also on the upper and lower measurement limits of capacitance measurement circuit [66].

3.2.3.3 Length of Electrodes

The total electrode length (L_t) should be at least equal to the diameter of the vessel/pipe. Commonly the length of electrodes is larger than the diameter of the sensor in order to avoid the fringe effect on the axial ends of sensor. An increase in L_t will further increase the sensitivity of the sensor.

The minimum (L_{min}) and maximum (L_{max}) length of measurement electrodes can be found by using equation (3-4) and (3-5) respectively [67]:

$$L_{\min} = \frac{C_{\min}}{K_2} \quad (3-4)$$

$$L_{\max} = \frac{C_{\max}}{K_1} \quad (3-5)$$

The total length of driven guard electrodes can be calculated by using equation (3-6):

$$L_t = L_m + 2L_g \quad (3-6)$$

where, C_{\min} is lower capacitance value, C_{\max} is higher capacitance value, K_1 is electrodes length between adjacent electrodes, K_2 is electrodes length between opposite electrodes, L_m is length of measurement electrode and L_g is length of driven guard electrode.

3.2.3.4 Driven Guard Electrodes

Yang (2006) suggested the usage of driven guard electrodes at both ends of the measurement electrodes and this arrangement is shown in Figure 3.7. When a measurement electrode is energised with the excitation signal then the two driven guard electrodes in the same axial line as the excitation electrode also receive the signal, while all others kept at virtual ground. This will prevent from the fringe effect, and hence shorter measurement electrodes may be used [64].

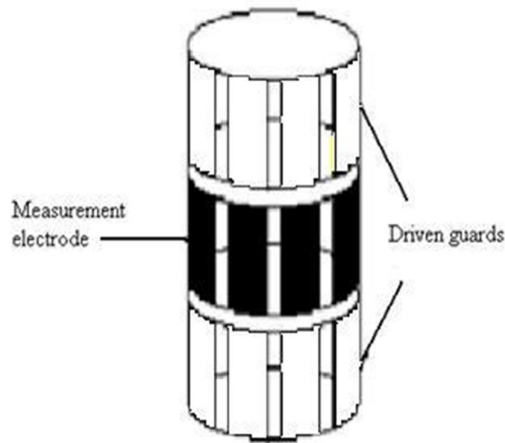


Figure 3.7: Layout of Driven Guard Electrodes [64].

3.2.3.5 Earthed Screens

An earthed screen must be placed in an ECT sensor in order to reduce the effects of extraneous signals and variations in the stray capacitance to earth; otherwise it will disturb the measurements. It is common to use the earthed end screens at both ends of the measurement electrodes, which can reduce an external noise as shown in Figure 3.8. Earthed radial screens are also used to reduce the standing capacitance between two adjacent electrodes. This method was also proposed by Yang (2010) [61].

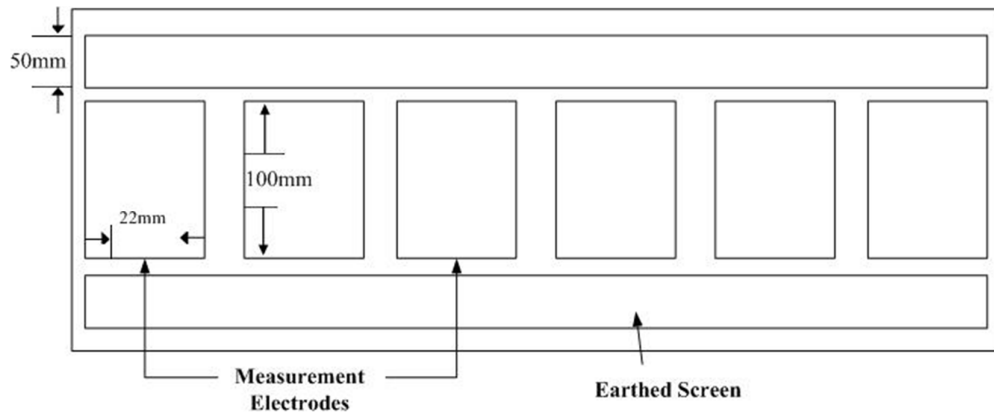


Figure 3.8: ECT Sensor with Earthed Screen at Both Ends.

3.2.3.6 Sensor Simulation using COMSOL

The numerical analysis of the electrical field of the sensor and calculations of the capacitance matrices were performed by using the FEM software i.e., COMSOL Multiphysics. ECT uses electrical field excitation; typically the measurement frequency of an ECT system is in the Mega Hertz (MHz) range. Therefore, the problem can be modelled as electrostatic [4]. The creation of a capacitance sensor model in FEMLAB® aims to obtain a method from which numerical calculation can be carried out for the electric potential Φ in the space of the sensor. According to Flores (2005), it is considered as an intermediate step towards the capacitance calculation. The electrostatic field inside an ECT sensor can be calculated by solving the Poisson's equation which is given by equation (3-7) [68]:

$$\nabla \cdot [\varepsilon(x, y) \nabla \varphi(x, y)] = -\rho(x, y) \quad (3-7)$$

where, $\varepsilon(x, y)$ is the electrical permittivity distribution, $\varphi(x, y)$ is the electrical potential distribution and $\rho(x, y)$ is the charge distribution, which is the source of electrical field. The Poisson equation is a linear partial differential equation in terms of $\varphi(x, y)$. If there exist no space charge inside the pipeline, the inner potential distribution can be described with 2D-Poisson equation [6], [62];

$$\nabla \cdot [\varepsilon_0 \varepsilon_r(x, y) \nabla \varphi(x, y)] = 0 \quad (3-8)$$

where, ε_0 is permittivity constant of free space, ε_r is relative dielectric permittivity and ∇ is gradient operator. The boundary conditions are of Dirichlet type and when electrode i is excited, the voltage on this electrode is V , whereas all other electrodes, radial guards and external screen are kept at zero potential [68]:

$$\varphi = V \quad (\text{On the excitation electrode}) \quad (3-9)$$

$$\varphi = 0 \quad (\text{On all other conductors}) \quad (3-10)$$

The charge sensed by detecting electrode can be found by applying Gauss law using the following equation [68]:

$$Q = \oint_{\Gamma} \varepsilon(x, y) \nabla \varphi(x, y) \cdot n ds \quad (3-11)$$

where, Γ is a closed curve surrounding the detecting electrode and n is the normal unit vector along Γ . Using the charge Q at each receiver electrode, the electrical capacitance can be calculated as [58], [68]:

$$C = \frac{Q_{ij}}{\Delta V_{ij}} \quad (3-12)$$

where, ΔV_{ij} is the potential difference between the sender and the receiver electrode (i.e. electrode i and j).

3.2.4 ECT Models

3.2.4.1 Calibration and Normalisation

It is a common practice to calibrate an ECT sensor by filling it with two different reference materials. In order to obtain a full range of variation in the measured capacitance, it is filled once with lower permittivity material and then followed by a higher permittivity material. As they have different dielectric properties and permittivity value. This process may be called as “two-point calibration” [69]. When a high permittivity object is introduced into a lower permittivity background in the imaging area, the capacitance of the electrode pairs may change. An ECT system measures these capacitance changes and reconstructs a cross-sectional image from the measured data using an appropriate algorithm, for example, linear back projection algorithm (LBP). Once the ECT system has been calibrated, then it is ready to capture the image data. When data capture is begin, the capacitances between all electrodes pair are measured at high speed. These capacitance changes later are usually normalised [70].

Normalisation is commonly used to calibrate an ECT system quantitatively between fixed points. It is important for ECT data due to very small capacitance values. When a mixture of two dielectric materials is imaged, an ECT system is calibrated by measuring two reference sets of inter-electrode capacitances. The sensor is first measured empty i.e. using air to find the lower capacitance C_l having a lower permittivity limit, then it is completely filled with material having a higher permittivity limit to acquire the values for higher capacitance C_h . All consequent measured capacitance values C_m are then normalised to have values C_n because when capacitance values are involved they are always normalised between “0” (when the sensor fully filled with lower permittivity material) and “1” (when the sensor fully filled with higher permittivity material) as shown in the following equation (3-13) [69]:

$$C_n = \frac{C_m - C_l}{C_h - C_l} \quad (3-13)$$

where, C_n is the set of normalised inter-electrode capacitances, C_m is the measured capacitance of the mixture flowing through the pipe; C_l is the measured capacitance when the sensor fully filled with lower permittivity material and C_h is the measured capacitance when the sensor fully filled with high permittivity material.

The pixel values in the permittivity image are also normalised, so they have the value “0” for lower permittivity material and “1” for the higher permittivity material. There are some benefits in utilisation of normalised values of quantities, such as [60]:

- i. Different ranges of capacitance, permittivity and pixel measurements are reduced to a single measurement range i.e. from 0 to 1.
- ii. Effect of measurement errors like offset and drift are eliminated.
- iii. The calibration of sensor becomes easy.

3.2.4.2 Distribution/Permittivity/Capacitance Models

ECT systems use the ‘raw capacitance data’ as measured from the sensor to calculate the normalised capacitance C_n as indicated in equation (3-13). Using the normalised capacitance can reduce the systematic errors in the measurement system. The capacitance measured depends on the relative permittivity of the materials between the electrodes. It depends on the distribution/permittivity models used to characterise the materials in the sensor cross-section.

The raw data obtained from these measurements are analyzed by applying distribution models which will result in normalised and measured capacitance values for 12-electrode measurements. The distribution models used are the *series*, *parallel*, *Maxwell* and *combined* model [66], [71]. The need for these different sensor models can be better understood by having a look at the Figure 3.9, which gives an insight into the problem and tells the usage of these models. It consists of simple parallel

plate capacitance cell containing two different dielectric materials, one is air and other is water (for this case). Figure 3.9 (a) and (b) shows the cell half-filled with the dielectric material but with two different distributions, Figure 3.9 (c) indicates that the cell completely filled with a dielectric constant k and Figure 3.9 (d) illustrates the distribution of materials in two ways within a capacitance cell. The more detailed information about these models is also given in Appendix ‘A’.

(a) *Series Model*

If the distribution is layered vertically, as shown in Figure 3.9 (a), the capacitance increases in a non-linear manner. The capacitances measured between the electrodes will be constituted from component capacitances which are effectively connected in series. In this case, the reciprocal rule for adding up capacitances in series must be used to obtain the component permittivities and concentration from the measured capacitances [60]. The normalised and measured capacitances for series model are shown in equation (3-14) and (3-15) respectively [71]:

$$\zeta = \frac{\frac{1}{C_m} - \frac{1}{C_l}}{\frac{1}{C_h} - \frac{1}{C_l}} \quad (3-14)$$

$$C_m = \frac{1}{\frac{\zeta}{C_h} + \frac{1-\zeta}{C_l}} \quad (3-15)$$

where, ζ is the fraction of the higher permittivity object using the Series model, C_m is the measured capacitance of the mixture flowing through the pipe, C_l is the measured capacitance of when the sensor is full with low permittivity material and C_h is the measured capacitance when the sensor is full with high permittivity material.

(b) *Parallel Model*

If the distribution is layered horizontally, as shown in Figure 3.9 (b), the capacitance of the cell increases linearly with the proportion of dielectric materials present. When the two dielectric materials exist as permittivity layers between the two electrodes, then two component capacitances are effectively connected in parallel between the electrodes. The sum of these capacitances will therefore accurately reflect the relative proportions (or concentration) of the 2 materials present. In this case, the mixture concentration is found by assuming that the dielectric materials combine to form two capacitances in parallel [60]. The equations for the normalised and measured capacitances using the parallel model are shown in equation (3-16) and (3-17) respectively [71]:

$$\lambda = \frac{C_m - C_l}{C_h - C_l} \quad (3-16)$$

$$C_m = (1 - \lambda)C_l + \lambda C_h \quad (3-17)$$

where, λ is the fraction of the higher permittivity object using the Parallel model, C_m is the measured capacitance of the mixture flowing through the pipe, C_l is the measured capacitance of when the sensor is full with low permittivity material and C_h is the measured capacitance when the sensor is full with high permittivity material.

(c) *Maxwell Model*

The third model which is a combination of two basic series and parallel distribution models was developed by *Maxwell* in the 19th century. The physical layout for this particular model is shown in Figure 3.9 (c). The equations for normalised and measured capacitances for *Maxwell* model are shown in equation (3-18) and (3-19) respectively [71]:

$$\phi = \frac{(\varepsilon_m - \varepsilon_l)(2\varepsilon_l + \varepsilon_h)}{(\varepsilon_h - \varepsilon_l)(2\varepsilon_l + \varepsilon_m)} \approx \frac{C_m - C_l}{C_h - C_l} \frac{2C_l + C_h}{2C_l + C_m} \quad (3-18)$$

$$\varepsilon_m = \varepsilon_l \frac{2\varepsilon_l + \varepsilon_h + 2\phi(\varepsilon_h - \varepsilon_l)}{2\varepsilon_l + \varepsilon_h - \phi(\varepsilon_h - \varepsilon_l)} \quad (3-19)$$

where, ϕ is the fraction of the higher permittivity object using the Maxwell model, C_m is the measured capacitance of the mixture flowing through the pipe, C_l is the measured capacitance of when the sensor is full with low permittivity material, C_h is the measured capacitance when the sensor is full with high permittivity material, ε_l is the lower permittivity, ε_h is the higher permittivity and ε_m is the permittivity of measured material.

(d) *Combined Model*

The forth model is a combination of all the previous three models. The physical arrangement of this model is represented in Figure 3.9 (d). The normalised and measured capacitance equations that categorized it as a combined model are shown in equation (3-20) and (3-21) respectively [71]:

$$\delta = \alpha \frac{(C_m - C_l)}{(C_h - C_l)} + (1 - \alpha) \frac{\frac{1}{C_m} - \frac{1}{C_l}}{\frac{1}{C_h} - \frac{1}{C_l}} \approx \frac{C_m - C_l}{C_h - C_l} \frac{C_h - \alpha(C_h - C_m)}{C_m} \quad (3-20)$$

$$C_m = \alpha[(1 - \lambda)C_l + \lambda C_h] + (1 - \alpha) \frac{1}{\frac{\zeta}{C_h} + \frac{1 - \zeta}{C_l}} \quad (3-21)$$

where, δ is the fraction of the higher permittivity object using the Combined model, C_m is the measured capacitance of the mixture flowing through the pipe, C_l is the measured capacitance of when the sensor is full with low permittivity material and C_h is the measured capacitance when the sensor is full with high permittivity material.

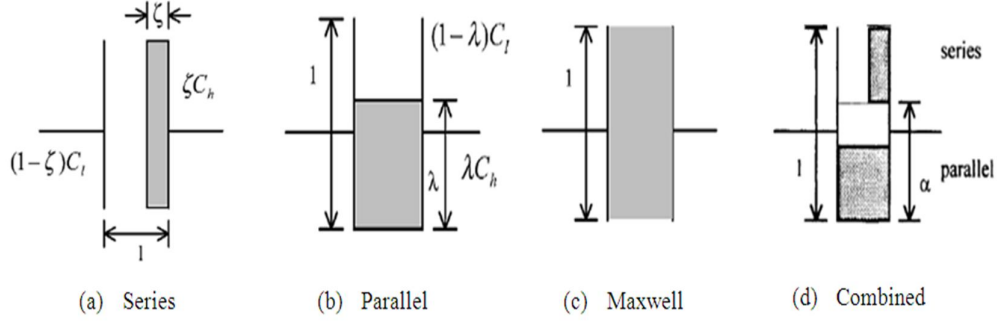


Figure 3.9: Distribution/Permittivity/Capacitance Models [71].

3.2.4.3 Image Reconstruction Algorithm

The subsequent stage of any tomographic system is to process the acquired data obtained from data acquisition unit by using an appropriate *image reconstruction algorithm*. Depending on the physical principle of a sensing system, the reconstructed image contains information on the cross-sectional distribution of the constituent parameter of an object. Once the change in capacitance has been measured from all possible electrode pairs, the next step is to reconstruct an image using the capacitance measurements to present the permittivity distribution. As the excitation source (voltage) for ECT system is generally of lower frequency (i.e. below 5 MHz), therefore, the electrical capacitance imaging system can be described by equations governing the *electrostatic field*, the Poisson equation [72]. For imaging of a dielectric object, multiple voltage-driven sensing electrodes are used on the periphery of the object.

It is a renowned phenomenon for electrostatic fields that whenever electric flux (or current) lines are encountered by an interface of different permittivities, the flux (or current) lines is deflected or bended. Therefore, different image reconstruction algorithms were developed for electrical capacitance tomography. The permittivity distribution related to capacitance measurement according to Poisson's equation is already mentioned in equation (3-7) above. The mutual capacitance between two pairs of electrodes is given by the ratio between stored charge and potential difference as shown in equation (3-22) [72]:

$$C_{ij} = \frac{Q_j}{\Delta V_{ij}} \quad (3-22)$$

where, C_{ij} is the mutual capacitance and ΔV_{ij} is the potential difference between electrodes i and j respectively obtained from equation (3-8) and Q_j is the charge on receiving electrode that can be found by using equation (3-11). Finally, equation (3-23) can be used for the calculation of mutual capacitance as [72]:

$$C_{ij} = \frac{1}{\Delta V_{ij}} \oint_{\Gamma} \varepsilon(x, y) \nabla \varphi(x, y) \cdot n ds \quad (3-23)$$

The equation (3-23) is known as the forward problem equation of ECT. The forward problem is to determine the inter-electrode capacitances from the permittivity distribution, e.g. by solving the partial differential equations, governing the sensing domain [6]. As there is no standard method exists for solving the reconstruction problem. Therefore, different researchers proposed different techniques. Image reconstruction for ECT system can be categorised into *iterative* and *non-iterative* techniques.

a) *Non-Iterative Algorithm*

The commonly used image reconstruction algorithm for non-iterative technique is the *Linear Back Projection (LBP)* algorithm. It is a simple procedure for reconstructing an image of an unknown permittivity distribution inside the sensor from the capacitance measurements. It was the first method used for this purpose and is still very commonly employed, despite the development of other methods (Yang 2003 [6]; Ortiz-Aleman *et al.* [73]). Although its reconstruction accuracy is not very good but it has the advantage of being fast and essentially a qualitative image reconstruction procedure [74]. It is well suited for fast dynamic processes like multiphase flow and widely used for online image reconstruction. The reconstruction in ECT is considered as a challenging task due to the soft field nature of the technique, in which the field distribution in the region of interest is dependent on the property distribution in a non-linear fashion [75].

The LBP algorithm shown schematically in Figure 3.10, where λ is the set of normalised changes in measured capacitance, S is the sensitivity map and E is the normalised permittivity distribution [76].

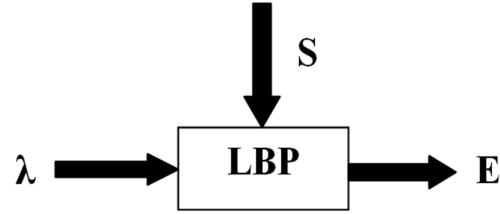


Figure 3.10: Non-Iterative LBP [76].

Prior to back-projection, the raw capacitance measurements corresponding to each electrode pair are normalised according to equation (3-24) [76]:

$$\lambda_{ij} = \frac{C_{ij}^m - C_{ij}^l}{C_{ij}^h - C_{ij}^l} \quad (3-24)$$

where, λ_{ij} is the normalised capacitance for electrode pair i - j , C_{ij}^m is the actual capacitance measured with that electrode pair, C_{ij}^l and C_{ij}^h are the capacitance when the sensor is filled with lower and higher permittivity material.

The basic LBP formula calculates the normalised grey level for each pixel as in equation (3-25) [71]:

$$G(p) = \frac{\sum_{i=1}^{N-1} \sum_{j=i+1}^N \lambda_{ij} S_{ij}(p)}{\sum_{i=1}^{N-1} \sum_{j=i+1}^N S_{ij}(p)} \quad (3-25)$$

where, $G(p)$ is the fraction of high permittivity material present at pixel p , λ_{ij} is the normalised capacitance between electrode pair i and j obtained from equation (3-24), $S_{ij}(p)$ is the sensitivity map of electrode pair i - j at p^{th} pixel and N is the number of electrodes of the ECT system.

b) Iterative Algorithm

When the LBP algorithm is used for online reconstruction only poor quality images can be obtained. In order to improve the image quality, iterative image reconstruction algorithms have to be used, the image quality has significant improvement but more computations are needed. Iterative algorithms are applied to ECT based on the measurement of capacitance values obtained from the permittivity distribution of the image, and then producing a new image using a difference between the measured capacitance and the calculated capacitance. This process is repeated until the minimum possible difference is achieved [6].

3.2.4.4 Voidage Calculation from ECT Measurements

The term “voidage”, “volume ratio” or “concentration” can be defined as the percentage of the volume of the sensor occupied by the higher permittivity material. The volume of the sensor is the product of the cross-sectional area of the sensor and the length of the measurement electrodes. The overall voidage of the contents of ECT sensor can be calculated by using two methods [60]:

- i. Using normalised pixel values in the reconstructed ECT image or;
- ii. Using the normalised capacitance measurements

All voidage values obtained from the ECT system are based on the assumption that the voidage is 100%, when the sensor is full of the higher permittivity material and is zero when the sensor is full of lower permittivity material.

a) Using Normalised Inter-electrode Capacitance Measurements

The average voidage can be obtained by using the normalised interelectrode capacitance measurements. It is done by summing all the normalised capacitance values for one image and dividing these by the sum of the normalised capacitances when the sensor is filled with higher permittivity material. This can be expressed in mathematical form as follows [60]:

$$VR = \frac{1}{N} \sum_{n=1}^N \left(\frac{C_n}{C_k} \right) \quad (3-26)$$

where, N is the total number of electrode pair measurements, C_n are the individual electrode pair normalised capacitances and C_k are the electrode pair capacitances when the sensor is full of the higher permittivity material.

b) Using Image Pixels

In the case of calculation from image pixels, the voidage is calculated by summing the values of the individual pixels in the ECT image for the required image frame and dividing it by the sum of these pixel values when the sensor is full of higher permittivity material [60]. Another method defined in section 2.4.3 can also be used to calculate the void fraction from pixels [35].

$$VR = \frac{1}{P} \sum_{i=1}^P \left(\frac{P_i}{P_k} \right) \quad (3-27)$$

where, P is the total number of pixels, P_i is the value of the i^{th} pixel and P_k is the value of the i^{th} pixel when the sensor is full of the higher permittivity material.

3.3 Differential Pressure (ΔP) Measurements

3.3.1 Theoretical Background

The scope of this research has also included differential pressure technique for the estimation of void fraction in air-water co-current bubble column. This technique was applied on the vertical test section of the test rig between two different pressure measuring ports. The measurement of void fraction by pressure difference method is simple, reliable, non-invasive and economical.

3.3.1.1 Single-Phase Flow

For steady, isothermal single-phase pipe flow, the momentum equation for a pipe segment provides the following expression for the pressure gradient [77]:

$$-\frac{dp}{dx} = \tau_w \frac{D_i}{A} + \rho g \sin \theta + \frac{G^2 d(1/\rho)}{dx} \quad (3-28)$$

where, A is the cross-sectional area of the pipe, D_i is the pipe inner diameter, τ_w is the wall shear stress, θ is the angle of the pipe and G the mass flux.

3.3.1.2 Two-Phase Flow

The theoretical background was proposed by Hills (1976) as well as by Merchuk and Merchuk (1981). In gas-liquid system, if liquid flow rate is small then, to a good approximation, the pressure drop can be wholly attributed to the hydrostatic head [80]:

$$\frac{dP}{dh} = -\rho_l g(1 - \varepsilon) \quad (3-29)$$

where, h is the axial coordinate pointing upwards.

The actual measurements can either be of the static pressure, or of the differential pressure using manometers or some kind of a pressure transducer. If dz is the height difference observed in a differential manometer, the following expression is [80]:

$$\rho_l g \frac{dh}{dz} = \frac{dP}{dz} + \rho_l g \quad (3-30)$$

If liquid flow rate is not negligible, then wall shear stress considered and also the effects of fluid acceleration due to void changes. In case of the two-phase flow, the final expression for the void fraction measurement includes all the terms as shown mathematically in equation (3-31) [80]:

$$\varepsilon = \frac{dz}{dh} + \frac{U_{sl}^2}{g} \frac{d}{dz} \left(\frac{1}{1 - \varepsilon} \right) + \frac{4\tau_w}{\rho_l D_i g} \quad (3-31)$$

where, U_{sl} is the liquid superficial velocity and D_i is the column inner diameter [80]. Equation (3-30) constitutes an implicit expression for the overall void fraction. The same approach has been adopted by Hills (1976) with the assumption of pseudo-homogenous two-phase mixture [78].

Figure 3.11 illustrates the principle of the differential pressure gradient method. When this technique is adopted, the terms corresponding to the friction and the acceleration effects are usually neglected. The lower the gas flow rate, the better is the approximation. This method can also be used to measure the average void fraction by installing a series of pressure taps situated along the column height [80].

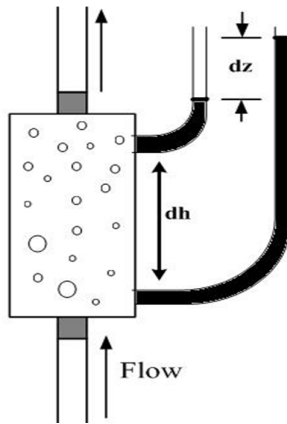


Figure 3.11: Principle for Holdup Measurements by Means of Differential Pressure.

3.3.2 Mathematical Description

This technique was applied by many previous researchers to determine or compare the void fraction measurements (C.Tang *et al.* 2006, E.Camarasa *et al.* 1999). In applying the pressure difference method, manometers were initially installed along the multiphase flow columns to measure the pressure signals (N.D.Hlaing *et al.* 2007). Recently, pressure transducers have been used and they are usually mounted to the column wall so that the disturbance to the flow caused by the pressure transducers is minimized. The technique assumes that the average differential pressure measurement in a vertical test section of a two-phase flow system is the sum of the static pressure drop (elevation head) Δp_{static} , momentum pressure drop (acceleration) Δp_{mom} , and the frictional pressure drop Δp_{frict} [82]:

$$\Delta P_{total} = \Delta P_{friction} + \Delta P_{acceleration} + \Delta P_{static} \quad (3-32)$$

Void fraction plays an important role in pressure drop calculation and also in flow pattern determination. All the four components of pressure drop directly or indirectly depend on the void fraction. In most cases, the acceleration and frictional terms can be neglected at low liquid velocities. Generally for air-water two-phase flows the acceleration term can be neglected. If the system is isothermal or adiabatic, and no expansion or phase change occurs, then the resultant differential pressure measurement between two pressure taps is the sum of gravitational component.

In general, the placement of differential pressure transducers allowed the measurement of two-phase pressure drop across the test section. However, this technique requires continuous monitoring (purging) of the pressure tapping lines so that they are filled with one of the phases (water) only. An easy penetration of another phase (air) often takes place and may cause a major source of error. Therefore, a bleed system accompanied so that the air can be purge out regularly to ensure the lines were filled with only water all the time.

Figure 3.12 indicates the differential pressure setup for evaluation of void fraction (holdup). Assuming one-dimensional isothermal flow, steady-state, constant cross-section, negligible mass transfer between the gas and liquid phases, and constant properties in a cross-section and the flow can be modelled as a pseudo-homogenous two-phase mixture.

C.Tang *et al.* (2006) proposed a following expression for vertical gas-liquid co-current flows to determine void fraction in a bubble column which will also be used in the current study to determine it by using equation (3-33) [7]:

$$\lambda_g = 1 - \frac{\Delta p}{\rho g \Delta h} \quad (3-33)$$

where, Δp is the difference of static pressure between two sensors placed at a distance h , h is the distance between the tappings, g is the acceleration due to gravity, ρ is the density and λ_g is the void fraction.

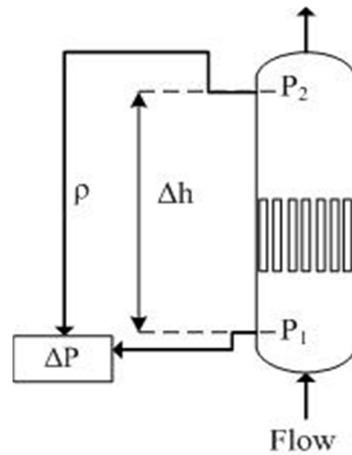


Figure 3.12: Schematic of the Differential Pressure Method Arrangement.

3.4 Summary

An ECT system and sensor have a wide usage and applications in the process industry as well as in medical field. The chapter has also discussed capacitance and permittivity models of ECT system. This system can be used to obtain images of the distribution of permittivity inside ECT sensors for any arbitrary mixture of different dielectric materials. However, an important application of ECT is viewing and measuring the spatial distribution of a mixture of two different dielectric materials (a two-phase mixture). For a two-phase mixture, ECT can be used to measure the spatial distribution of the composite permittivity of the two materials inside the sensor. From this permittivity distribution, it is possible to obtain the distribution of the relative concentration (volume ratio) of the two components over the cross-section of the vessel. Voidage calculations from ECT normalised capacitance and pixel measurements were also presented briefly. The chapter also covers differential pressure measurement i.e. another non-invasive technique that can measure the void fraction in bubble columns. The description for this technique was divided into two parts, initially it was defined for single-phase flows and then its application was extended for the description of two-phase flows. It was recommended to use a series of pressure taps along the column height which would enable the measurement of sectional holdup in the system.